Simulated and Experimental Characteristics of Analysis Techniques for ZrCuAlNi/AlOx/Al Metal-Insulator-Metal Tunnel Diodes

June 3, 2012

Abstract

This project examines the results of current-voltage conduction mechanism analysis techniques simulated under assumed conduction conditions. Thermionic emission and Fowler-Nordheim tunneling conditions are simulated and analyzed. The resulting plots show how devices behave under different condition mechanisms. The effects of different conduction mechanisms on the results of various analysis techniques are also observed. In addition, the impact of instrument resolution or signal noise flooe are also evaluated, and provide insight on which characteristics of the analyses are artifacts due to such noise floors. Simulated behaviors are also compared with experimental results of ZrCuAlNi/AlOx/Al metal-insulator-metal (MIM) devices in order to observe differences between simulated and measured behaviors.

Keywords: Device Simulation, MIM Tunneling Diode, Fowler-Nordheim Tunneling, Schottky Emission, Poole-Frenkel Effect.

Contact: tanche@onid.orst.edu

Simulated and Experimental Characteristics of Analysis Techniques for ZrCuAlNi/AlOx/Al Metal-Insulator-Metal Tunnel Diodes

by Cheng Tan

A PROJECT

submitted to

Oregon State University

University Honors College

in partial fulfillment of

the requirements for

the degree of

Honors Baccalaureate of Science

in

Electrical and Computer Engineering

Presented May 31st, 2012

Commencement June 2012

Honors Baccalaureate of Science in Electrical and Computer Engineering project of Cheng Tan presented on May 31st, 2012.

APPROVED:

Mentor, Dr. John F. Conley Jr. representing Electrical and Computer Engineering

---

Committee Member, Dr. Thomas K. Plant representing Electrical and Computer Engineering

---

Committee Member, Dr. Terrance O' Regan representing Army Research Lab

---

Chair, Dr. Terri S. Fiez representing Electrical and Computer Engineering

---

Dean, Dr. Dan Arp, University Honors College

I understand that my project will become part of the permanent collection of Oregon State University, University Honors College. My signature below authorizes release of my project to any reader upon request.

Cheng Tan, Author

Acknowledgments

I would like to acknowledge the supervision of Dr. John Conley, Jr. I also thank Dr. Terrance O' Regan for his original code. I must acknowledge Nasir Alimardani and William Cowell III for the devices in which models were based on. Addtionally, I would like to thank Matthew Chin, Nick Landau, and Dr. Anthony "Glen" Birdwell at Army Research Lab for their support and relevant discussions. Ben Lampert and Chad Layne are thanked for their general support as well as discussions. In particular I would like to acknowledge Dr. Thomas Plant for his support.

I am grateful to all of my friends from Oregon State University and Army Research Lab for their support. I must also recognize the support I have received my family throughout the process, especially from my mother.

I recognize that this research would not have been possible without the assistance of Army Research Lab, Oregon State University Department of Electrical Engineering and Computer Science, and the College of Engineering at Oregon State University, and express my utmost gratitude.

Contents

List of Figures

1 Introduction

Metal-Insulator-Metal (MIM) tunnel junctions have possible applications such as high speed transistors, infrared (IR) devices, and liquid-crystal display (LCD) backplanes[1]. Electron transport in MIM junctions can be described by various current-voltage mechanisms such as Fowler-Nordheim tunneling[2], Frenkel-Poole emission[3, 4], and Schottky emission[3, 5]. These different mechanisms have elicited a variety of analysis methods of MIM junctions. While there are many techniques and methods to extract information of device mechanisms, data analysis is often made difficult by the lack of information on how they behave when the conditions deviate from the ideal behaviors assumed. This thesis attempts to provide insight on a few of these methods via simulation and comparison with experimental results. The simulated current-voltage behavior used in this report is a combination of simulated Schottky emission[5] and a modified version of Simmons' tunneling model[6].

2 Fabrication and Experimental Setup

Shown in Figure 1 is the device structure tested in the experiment, which contained a sputtered ZrCuAlNi (ZCAN) bottom electrode M_1 with a 10 nm atomic layer deposited (ALD) blanket of amorphous AlOx dielectric insulating layer I and thermally evaporated Al as top electrode contact M_2. The devices were fabricated by Nasir Alimardani and William Cowell of Oregon State University[14, 15]. Contact to the bottom electrode was made by scratching through the AlOx and applying a layer of In solder to the scratched surface. Device characteristics were measured at room temperature using an Agilent 4155C Semiconductor Parameter Analyzer in a blackbox probe station equipped with tungsten tips. I-V measurements were conducted by holding the bottom electrode constant as ground while sweeping the bias voltage of the top electrode. The voltage was swept to the target negative or positive bias from 0 V, and then reverse swept back to 0 V. The barrier heights of the device were experimentally determined to be 2.4 eV for the Al/AlOx interface and 3.2 eV for the ZCAN/AlOx interface via internal photoemission spectroscopy (IPS). Such barriers yields the energy band diagram found in Figure 2.

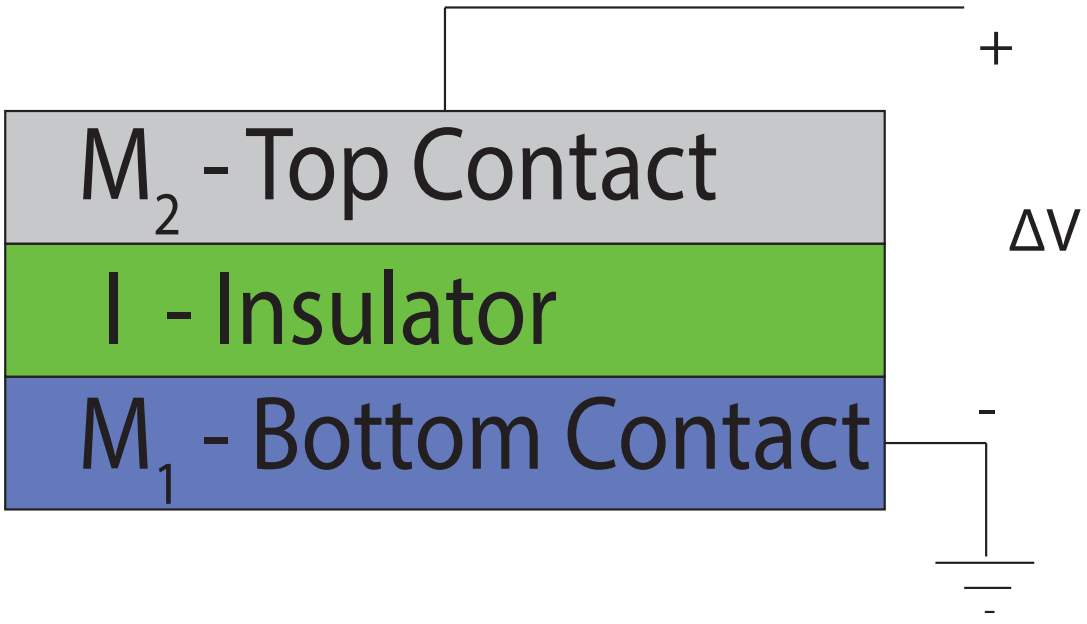

Figure 1: In the device structure tested, M_1, the bottom electrode (ZCAN) was held constant while a bias was applied to M_2, the top electrode (Al). The dielectric I in this device structure was 10 nm AlOx.

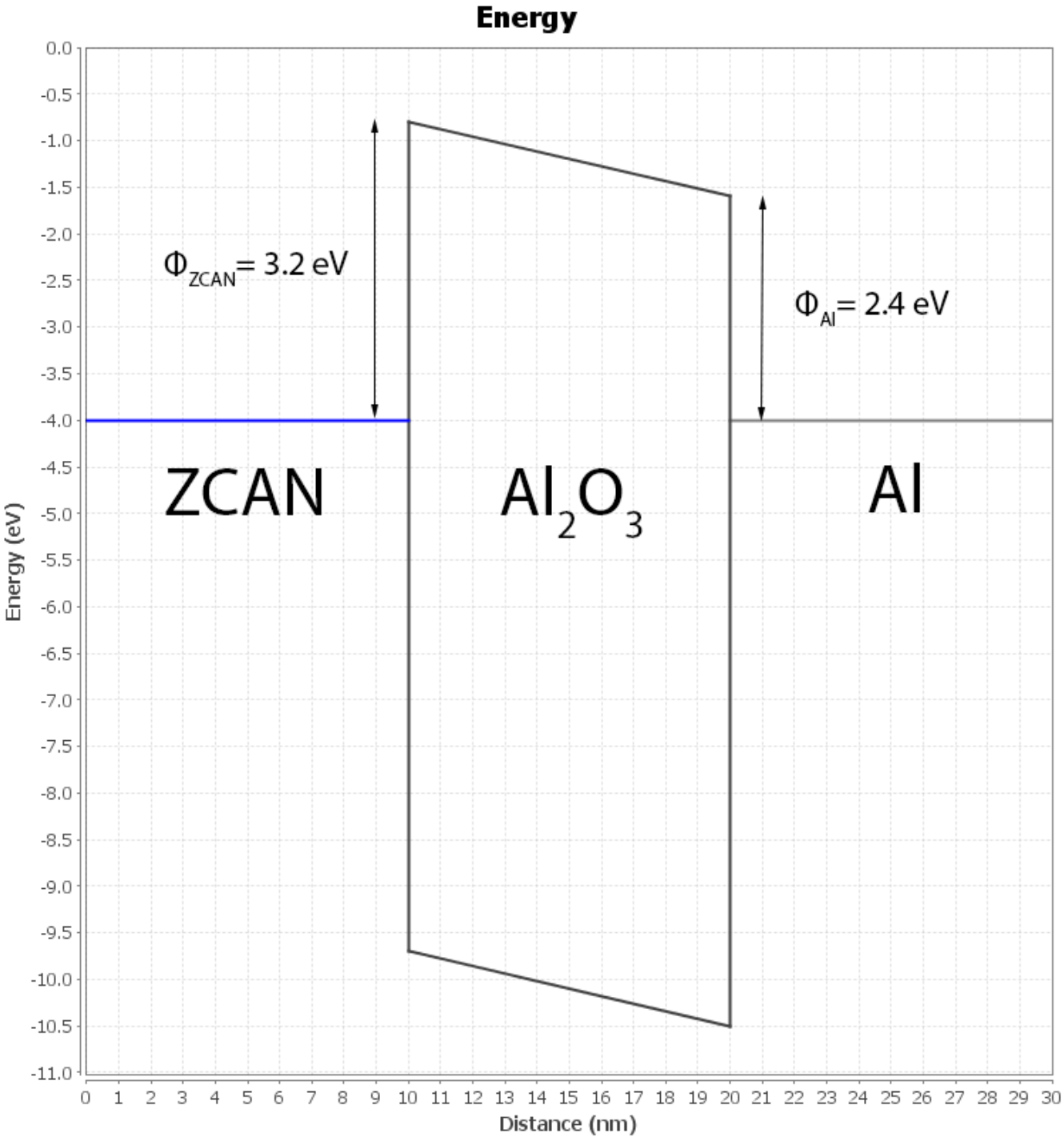

Figure 2: An energy band diagram of the device structure under flatband conditions, plotted with [7], which shows the 3.2 eV ZCAN/AlOx barrier and the 2.4 eV Al/AlOx Barrier.

3 Analyses and Simulations

3.1 Simulation Details

Current-voltage (I-V) simulations provided by Dr. O' Regan of U. S. Army Research Lab (ARL)[13] include the Simmons[6] model of Fowler-Nordheim tunneling[2] with image potential effects as well Schottky thermal effects[5]. The Poole-Frenkel effect was not simulated due to the complexity of trap densities and mobilities. Using the simulated model, additional work was done to simulate a noise floor of 50 pA by hard setting simulated currents lower than the noise floor equal to the noise floor. The 50 pA value was determined by the noise limits of the device measured. Using the I-V results simulated, a series of plotting analyses were done and compared to the analyses of the measured device. The specific methods are detailed in this section. The barrier values were chosen to be the experimental values shown in Figure 2, with all other parameters adjusted to fit the experimental I-V behavior. Additionally, to evaluate the various analyses methods under thermal effects dominated regimes, models were also run with energy barriers of 0.5 eV and 0.7 eV, with other parameters adjusted to ensure the simulation of thermal effects dominance.

3.2 Logarithmic Conductivity

Reported by Gundlach[8], the technique plots $\frac{d \ln J}{dV}$, or the logarithmic conductivity, as a function of V, where J is the current density and V is the applied voltage. The technique analyzes MIM tunneling dominated devices, in which the plot should show a characteristic maximum within 0.2 V of the voltage that corresponds to the Metal-Insulator barrier height in electron-volts (eV), which is the onset of Fowler-Nordheim tunneling through the triangular barrier. For devices simulated in this work, the Fowler-Nordheim tunneling onset is shown in Figures 3 A and 3 B. From the logarithmic conductivity plot, one can determine the apparent barrier height of the interface. The plot displays this characteristic independently of the effective mass and the thickness, though changes in these parameters do change the overall magnitude of the values.

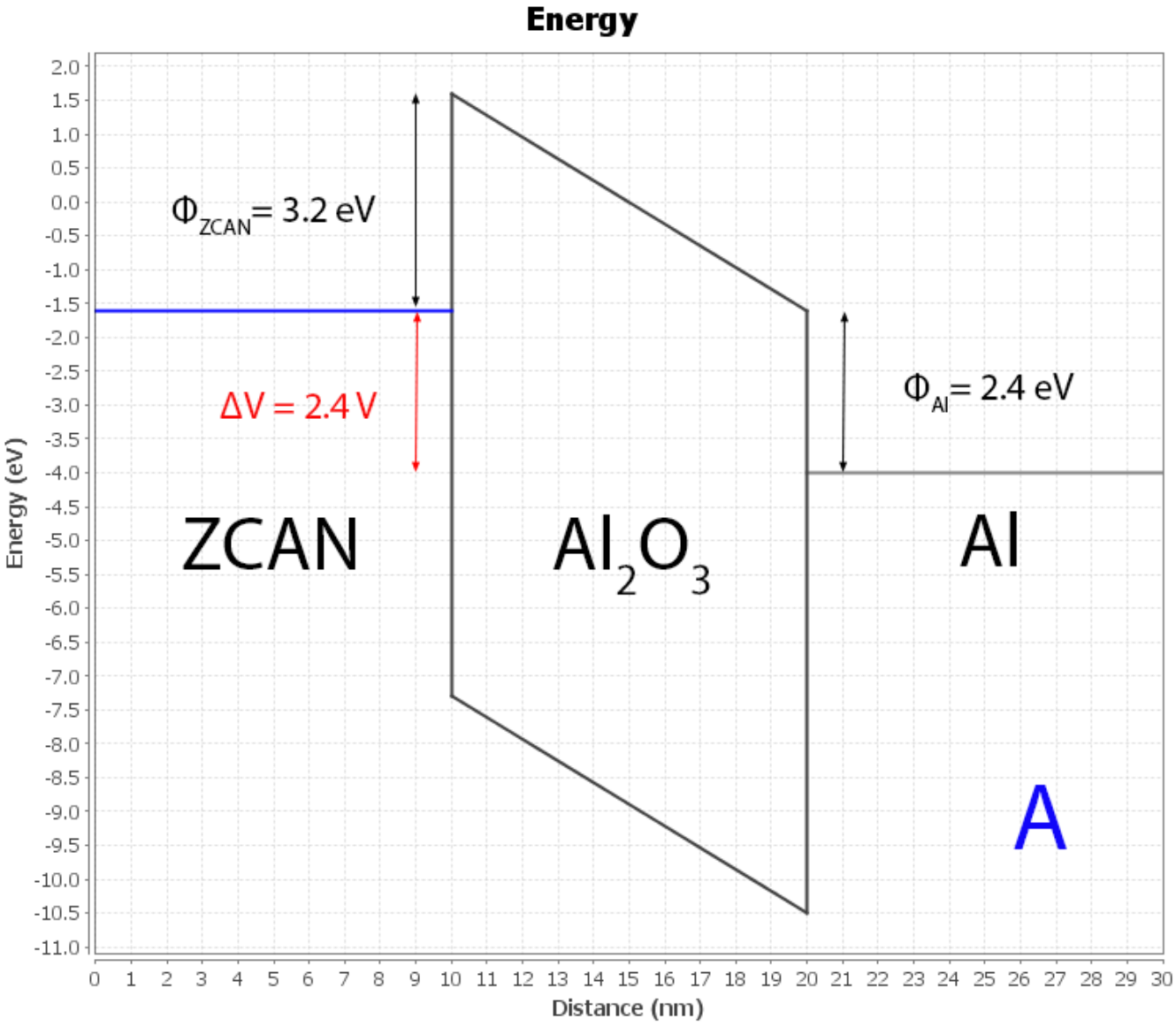
Energy
Φ ZCAN = 3.2 eV
ΔV = 2.4 V
Φ Al = 2.4 eV
ZCAN
Al2O3
Al
A
Energy (eV)
Distance (nm)

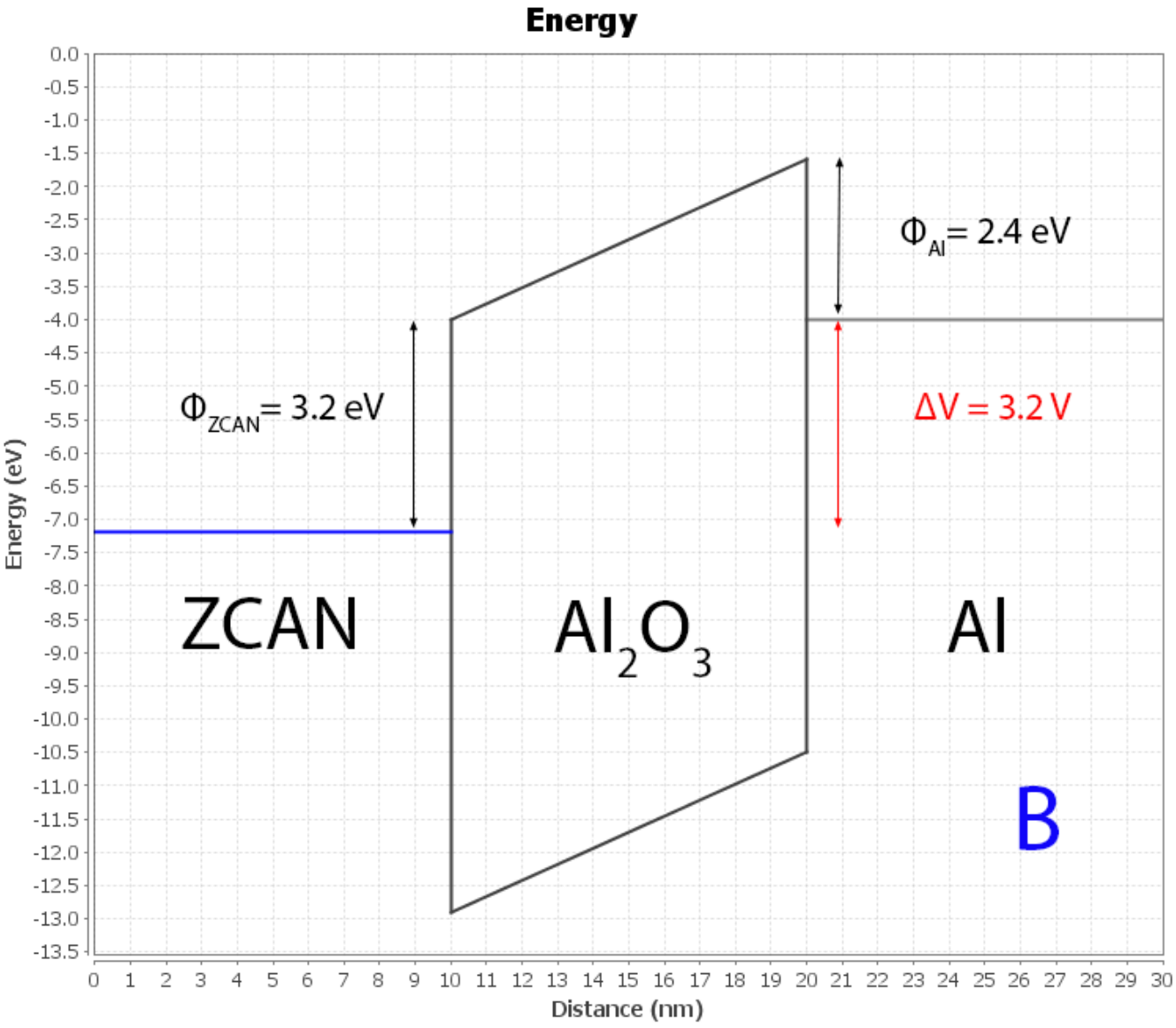

Figure 3: For the device structure evaluated, the expected onsets of Fowler-Nordheim tunneling are at A: 2.4 V and B: -3.2 V.

3.3 Thermal Effects

Two of the well-known thermally-affected mechanisms for MIM junctions are Schottky emission and Frenkel-Poole emission. Schottky emission, an electrode-limited conduction process, is the field-enchanced capacity of hot electrons to go into the conduction band of the insulator when the device operates at high temperatures. The operation is given as the Richardson-Schottky equation, which finds the current density as[3]:

$$J = \frac{4\pi m^* e k^2 T^2}{h^3} \exp\left(-\frac{\varphi_0}{kT}\right) \exp\left(\frac{\left(\frac{e^3 E}{4\pi\epsilon_0 \mathcal{K}}\right)^{1/2}}{kT}\right) \tag{1}$$

for devices where the electron mean free path is in the order of insulator thickness. In the above equation, m^* is the effective electron mass, e is unit of electronic charge, k is Boltzmann's constant, h is Planck's constant, φ_0 is the barrier height in electron volts, K is the high frequency dielectric, ϵ_0 is the absolute permittivity, and T is the temperature. Additionally, the conductivity of a Schottky emission dominated device is given as [9]:

$$\sigma = \sigma_0 \exp\left(\frac{\left(\frac{e^3 E}{4\pi\epsilon_0 \mathcal{K}}\right)^{1/2}}{kT}\right) \tag{2}$$

where σ is the conductivity $\frac{J}{E}$ and σ_0 is the zero-field conductivity.

In the Poole-Frenkel effect, a bulk-limited conduction process, the electrons move across the insulator via local traps and thermal fluctuations, and the current density for insulators with traps of ionization potential U is given by[3]:

$$J = e\mu N_c E \exp\left(-\frac{U}{kT}\right) \exp\left(\frac{\left(\frac{e^3 E}{\pi\epsilon_0 \mathcal{K}}\right)^{1/2}}{kT}\right) \tag{3}$$

where N_c is the carrier concentration and μ is the carrier mobility.The current density for insulators with shallow traps is given by:

$$J = e\mu N_c E \exp\left(-\frac{U}{kT}\right) \exp\left(\frac{\left(\frac{e^3 E}{\pi\epsilon_0 \mathcal{K}}\right)^{1/2}}{2kT}\right). \tag{4}$$

According to equations 2, 3, and 4, when $\ln\sigma$ is plotted against $\sqrt{E}$, a linear relation is observed if either the Poole-Frenkel effect or the Schottky effect is present in the MIM junction. From the linear plot, the high frequency dielectric constant K can be calculated with the slope β_{PF} from the following[9]:

$$\beta_{PF}=\frac{1}{kT}\left(\frac{e^3}{\pi\epsilon_0\mathcal{K}}\right)^{1/2} \tag{5}$$

for bulk limited conduction and:

$$\beta_S=\frac{1}{kT}\left(\frac{e^3}{4\,\pi\epsilon_0\mathcal{K}}\right)^{1/2} \tag{6}$$

for electrode limited conduction with slope β_S. In addition, by plotting $\ln J$ against $\sqrt{E}$ as per equation 1, one can identify the voltage range over which the the MIM device switches from operating in the electrode limited contact to bulk limited contact. The plot shows an elbow in the curve, above which there is bulk limited conduction, and below which it is electrode limited conduction. This allows for the distinction between the two prominent thermal effects in MIM devices if it existed. In the case of the simulated model, no elbow should be shown since only one conduction mechanism is simulated. [10]

Additionally, from the thermionic equations, it can be shown that for a device dominated by Schottky behavior, a plot of $\ln\frac{J}{T^2}$ vs. $\frac{1000}{T}$ at a set bias should yield a linear behavior. Since the simulations involved use strictly Schottky models for thermal effects, the behavior shown in the analyses are expected to be the result of the interactions between Schottky emission and electron tunneling conduction mechanisms and should reflect this.

3.4 Fowler-Nordheim Tunneling

Fowler-Nordheim tunneling in MIM devices is a mechanism at high biases in which electrons tunnel from the electrode fermi band into the conduction band of the insulator, before traveling to the opposite electrode via electric drift. The simulated current in this work is given by equation 7[13, 6].

$$J=\frac{e}{2\pi h(\beta\Delta s)^2}\left\{(\bar{\varphi}\exp(-\frac{4\pi\beta\Delta s}{h}(2m^*\bar{\varphi})^{1/2})-(\bar{\varphi}+eV)\exp(-\frac{4\pi\beta\Delta s}{h}(2m^*(\bar{\varphi}+eV))^{1/2})\right\} \tag{7}$$

Where the mean barrier $\bar{\varphi}$ is given as:

$$\bar{\varphi} = \frac{1}{\Delta s} \int_{s_2}^{s_1} \varphi(x)\ dx \tag{8}$$

The variables s_1 and s_2 are the positions of the metal-insulator interfaces, and the tunneling distance isΔs=$s_1 - s_2$. In equation 7, β is a correction factor, h is Planck's constant, V is the bias applied, e is the electron charge, and m^* is the effective electron tunneling mass.

The Fowler-Nordheim analysis plots the $\ln\frac{J}{E^2}$ plotted against $\frac{1}{E}$, where J is the current density and E is the electric field, the plot is shown to be linear if Fowler-Nordheim tunneling is dominant[11]. Murakami has proposed plotting $\frac{d\,ln\,J}{d\,ln\,E}$ vs. E in order to identify the mechanisms within the I-V response. A clearly defined peak identifies Fowler-Nordheim tunneling dominated response and the lack of one identifies the response as thermal effect dominated [12]. Anything in between is a composition of the two, with the ratios extractable via additional simulations.

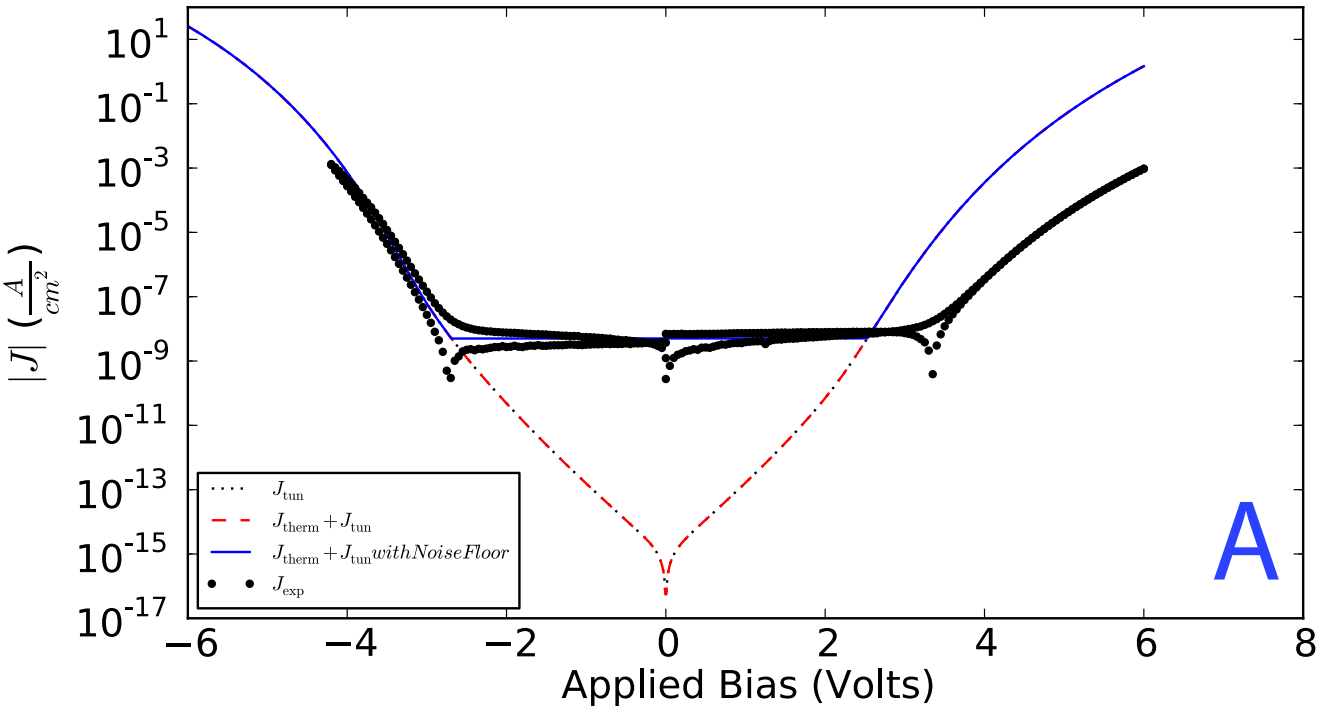

4 Results and Discussions

4.1 Current-Voltage Behavior

Figure 4 shows the simulation of the I-V characteristics using a barrier height of 3.2 eV for the M_1/ I (ZCAN/AlOx) interface and a barrier height of 2.4 eV for the M_2/ I (Al/AlOx) interface, a high frequency dielectric constant of 1.3, an insulator thickness of 10 nm, and an effective electron tunneling mass at 10% of the electron mass at a temperature of 298 K. The barrier height values and the device thickness are the experimentally determined results while the dielectric constant and effective electron tunneling mass were fitted via the simulation. The results are plotted in Figure 4 on an absolute value logarithmic plot. Using this set of simulation parameters, there is a high correspondance for the simulated and experimental data on the negative bias while there appears to be an offset for the positive bias. A potential explanation is the interference from a native ZrOx layer at the ZCAN/AlOx interface, which may cause deviations from the modeled positive bias behavior[15]. The difference between the two simulations with and without the noise floor are shown in behavior of the current response at lower biases, this behavior is also seen in the experimental results, with more fluctuation in the noise measured.

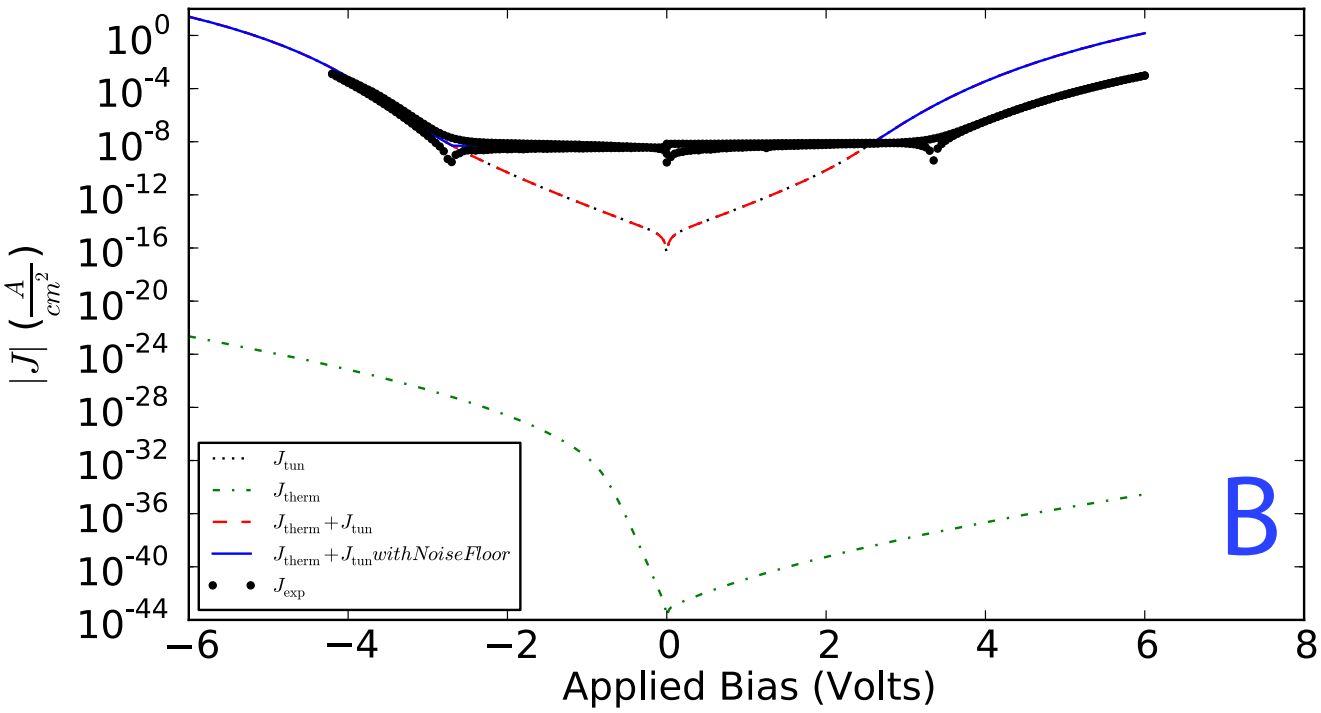

Figure 4: Simulated and experimental I-V response of a ZCAN/10 nm AlOx/Al MIM device A without the thermal effects current shown and B with the thermal effects current shown. The green shows the thermal effects current simulated at 298 K in B, while the red shows the simulated Fowler-Nordheim tunneling current, which also happens to the total current in this scenario, due to tunneling being the dominant mechanism. The blue shows the behavior of simulation with the noise floor on the log (I) vs. V plot, which reflects the noise floor of the experimental result. The dips in the experimental data are due to the displacement current in the reverse sweep of the devices, and are shown as sudden peaks or dips in the results of many analysis techniques in this work.

4.2 Logarithmic Conductivity

In Figure 5, the logarithmic conductivity analysis is done for both simulations as well as the experimental data by plotting $\frac{d \ln J}{dV}$ vs. V. In the results, the noise floor obfuscates the analysis process and the maximum that is observed can be artificial. This is due to the actual expected value being within the noise level, which renders the current signal unobservable. When the current measured is above the noise floor, a sharp peak is observed in the simulations due to the remnant behavior. In the experimental results, however, the peak is more gradual as the current rises above the noise floor. The created maximum can be easily mistaken for the expected peak, leading to incorrect barrier approximations. The observed asymptotes near the peak in the experimental results are due to the displacement current of the reverse voltage sweep back 0 V. Again, there is an offset between the simulations and the experimental data for the positive bias current response, a result of the I-V offset.

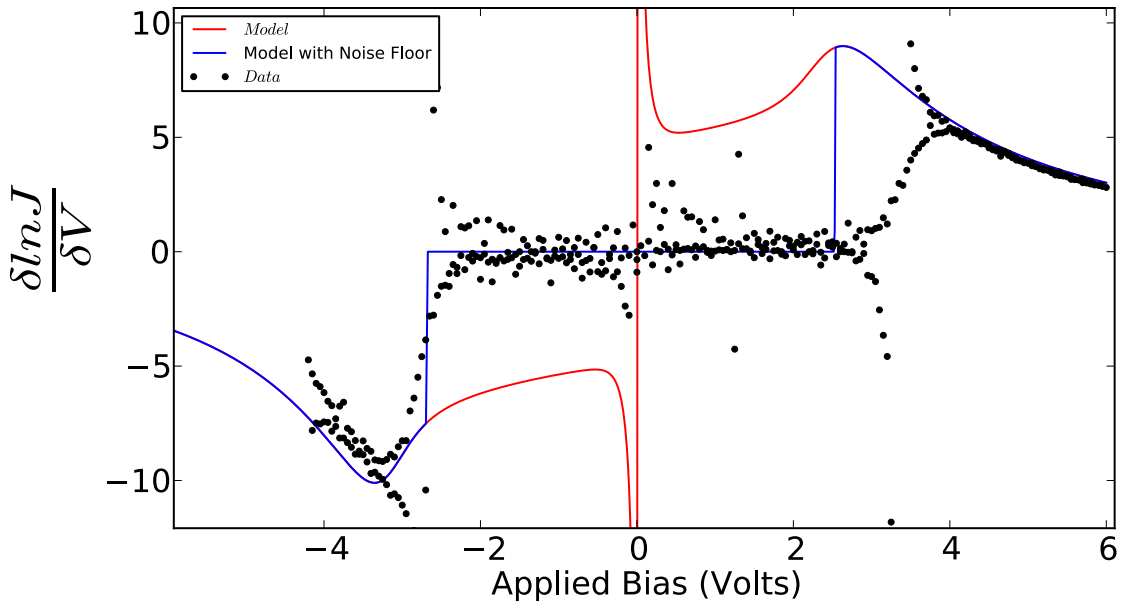

Figure 5: Simulated and experimental logarithmic conductivity analysis results. The red is the original simulated result, while the blue shows the effects of the noise floor as a sharp rise. In the experimental results, however, the transition out of the noise floor is shown as a gradual change, which can cause the resulting local maximum to be mistaken for the expected peaks.

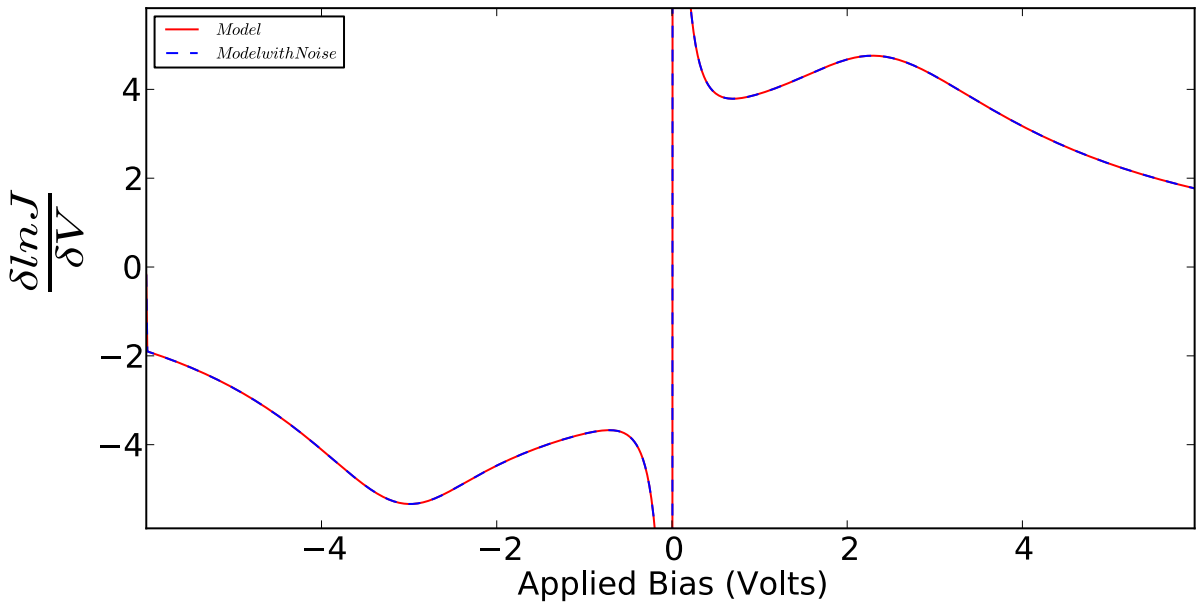

Figure 6: Simulated and experimental logarithmic conductivity analysis results with all parameters held constant except for thickness, which is changed to 2 nm. The red is the original simulated result, while the blue shows the effects of the noise floor as a sharp rise. In this plot, the two are the same since the reduced thickness has caused the current response to be higher than the noise floor, showing the entirety of the analysis.

In order to achieve a higher current response above the noise to measure the barrier height via this method, thinner devices achieve higher currents, as shown in Figure 6. Structures with lower barrier heights also have higher currents above the noise level, but can be more prone to the temperature variations outlined in section 4.5.

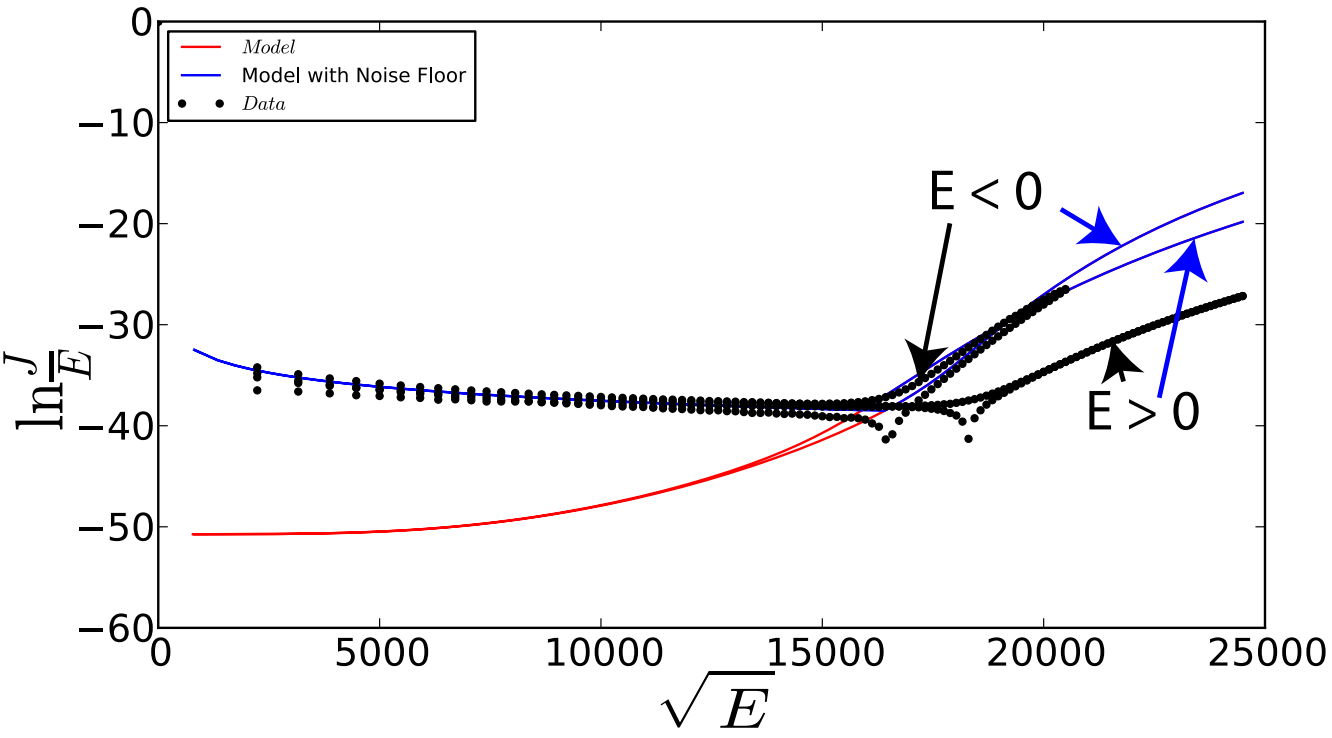

Figure 7: Simulated and experimental results of $\ln\frac{J}{E}$ vs. $\sqrt{E}$. The red shows the original simulated result while the blue shows the simulation with a noise floor. The black shows the analysis of experimental data. A significant offset exists between the experimental and simulated results on the positive bias due to differences in the simulated vs experimental curves for that side. The noise floor introduces a deviating behavior that exists for lower biases, as well as a local minimum in the plot. Note how the region above the noise floor in the experimental analysis could be mistaken for linear behavior, due to Fowler-Nordheim tunneling and a lack of information of lower bias response.

4.3 Thermal Effects

Devices with smaller barrier heights see a larger dominance of thermal effects with an increase in temperature. In the case of the ZCAN/AlOx/Al device that was measured, large barriers on both interfaces can cause the thermal effects currents to be negligible at room temperatures. When $\ln\frac{J}{E}$ of the total current is plotted against $\sqrt{E}$ (both positive and negative biases are included), as shown in Figure 7, the result is a non-linear behavior that is also seen in the plot of $\ln J$ against $\sqrt{E}$, illustrated in Figure 8, which suggests that thermal effects are not the dominating mechanism in the device. Additionally, the noise floor adds an artificial plateau and elbow into the data at lower electric fields.

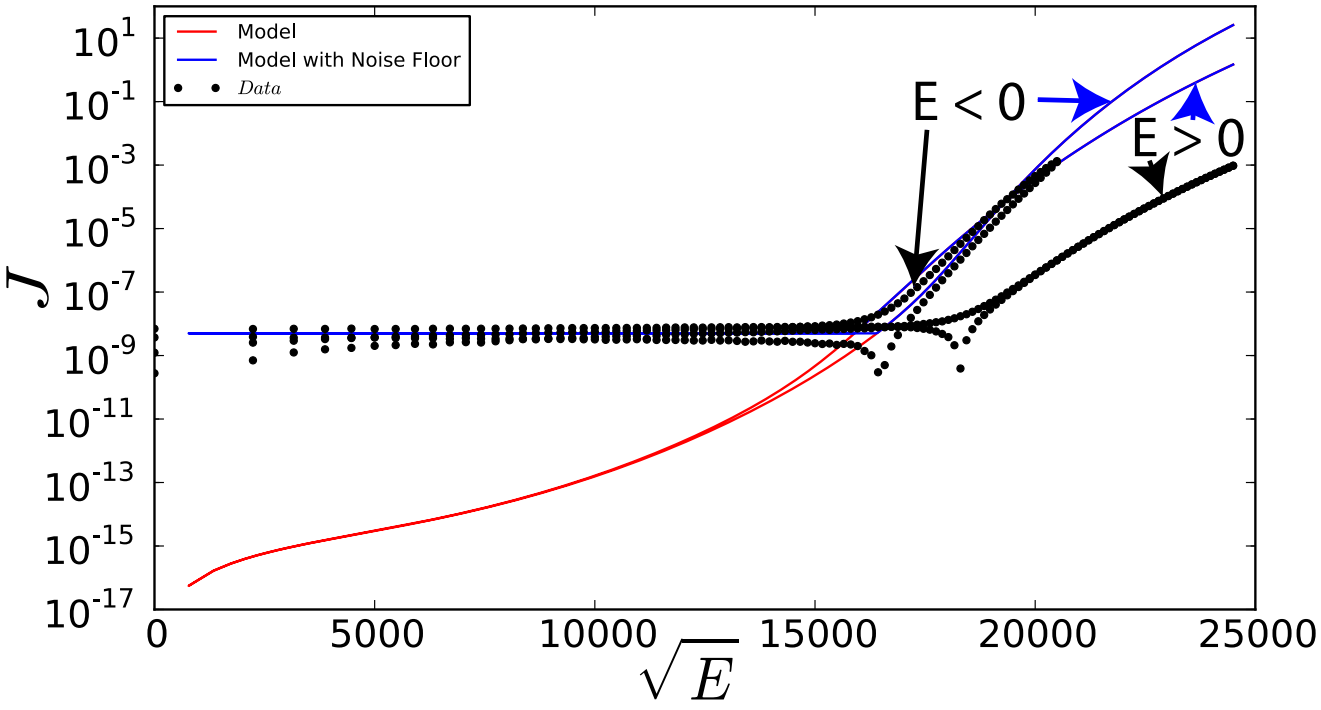

Figure 8: Simulated and experimental results of ln J vs. $\sqrt{E}$. The red shows the original simulated result while the blue shows the simulation with a noise floor. The black shows the experimental analysis. The behavior is very much like that of Figure 7, with similar offsets in the positive bias. Differences are caused by the noise floor, as the plateau shown here is perfectly flat, and the local minimum that was observed in Figure 7 is now shown to be an elbow in the plot. The region above the noise floor in the experimental analysis could be mistaken for linear behavior, due to Fowler-Nordheim tunneling and lack of lower bias information.

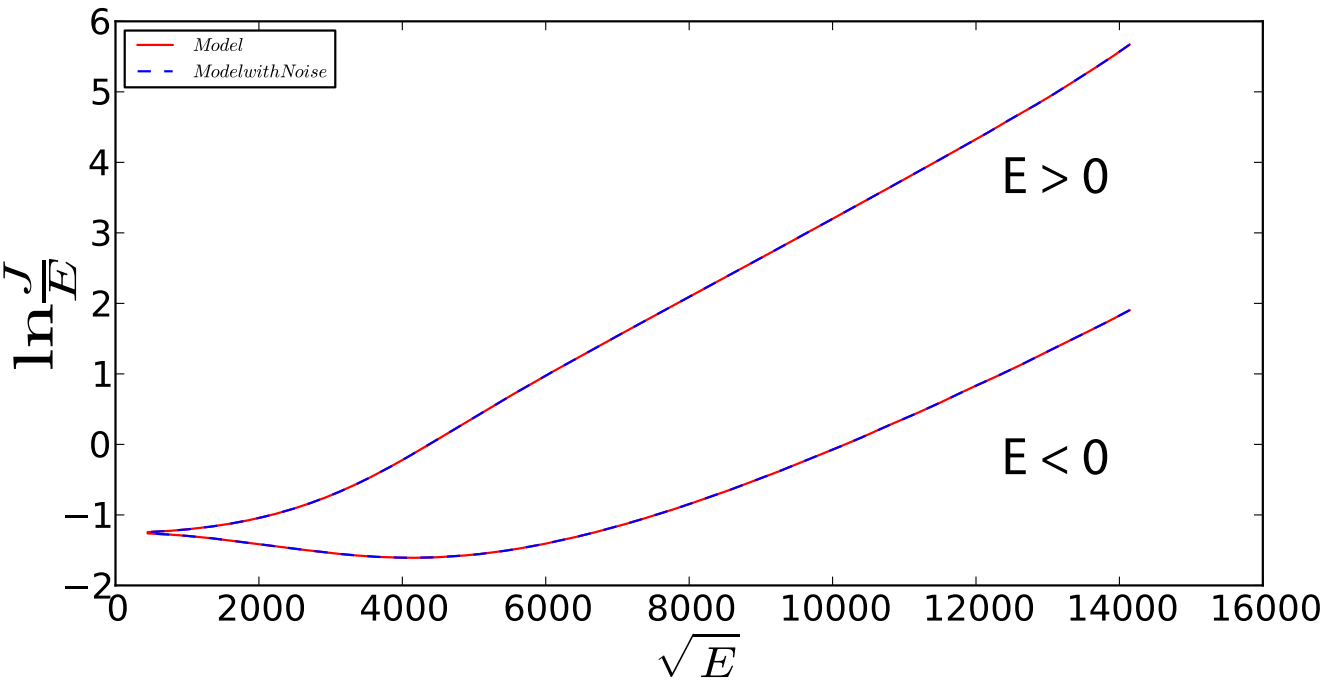

Figure 9: Simulated results of $\ln\frac{J}{E}$ vs. $\sqrt{E}$ in a thermal effects dominated simulation. The red shows the original simulated result while the blue shows the simulation with a noise floor. In this case, the two are overlapping due the current being above the noise floor. A linear behavior is shown for higher electric fields due to Schottky emission.

To demonstrate a device dominated by thermal effects, Figures 9 and 10 use 0.5 eV (M_1/I interface) and 0.7 eV (M_2/I interface) as barrier height values for a device at 500 K with an effective mass ratio of 1, parameters chosen to illustrate the behavior of a thermal effects dominated device, the resulting two plots show more linear behavior at higher electric fields, but the initial non-linear behavior should be taken into consideration during analysis. The lack of an elbow is expected, as only Schottky emission is simulated, but the response transition from the lower to higher applied fields as a result of the tunneling response may be mistakenly taken as an elbow for a transition between Schottky and Frenkel-Poole dominated conduction. Additionally, taking the slope via the linear extrapolation of the simulated results of the $\ln\frac{J}{E}$ vs. $\sqrt{E}$ produced a relative dielectric constant value of ~2, when the dielectric constant value used for simulation was actually 1.3, suggesting for deviations for the extracted dielectric constant even under thermal effects dominated conditions. The two analysis techniques share numerous similarities in behavior and purpose, as seen in the plots.

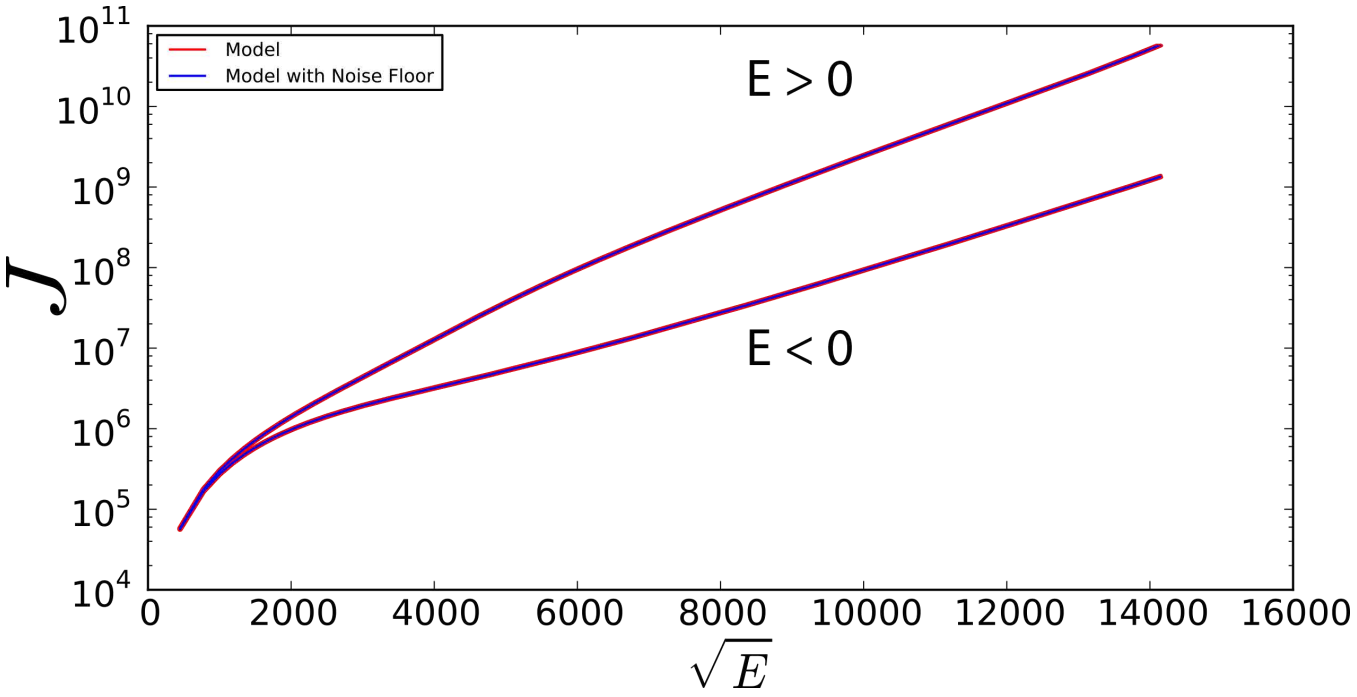

Figure 10: Simulated and experimental results of ln J vs. $\sqrt{E}$. The red shows the original simulated result while the blue shows the simulation with a noise floor. In this plot, the red and blue are overlapped. The behavior is linear similar to that of Figure 9 at higher biases, but the concavity of the overall behavior differs. It is difficult to distinguish if there is an elbow in the overall behavior.

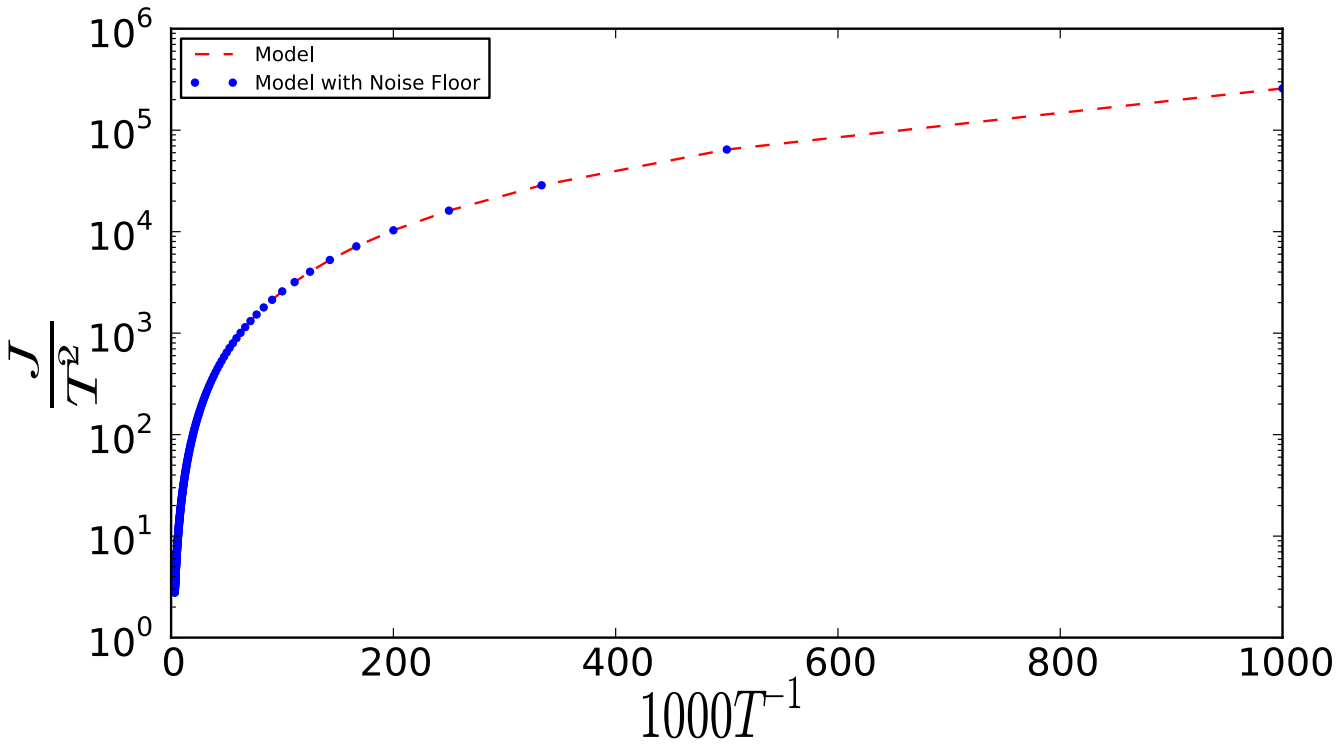

Figure 11: Simulated results of $\ln \frac{J}{T^2}$ vs. $\frac{1000}{T}$ at a bias of -6 V or an electric field of -6 MV/cm. The red shows the original simulated result while the blue shows the simulation with a noise floor. The behavior is not linear due to Fowler-Nordheim tunneling, since the variation of current varies little with changes in temperature.

By sweeping the temperature from 1 to 500 K, the resulting $\ln \frac{J}{T^2}$ vs. $\frac{1000}{T}$ plot was extracted at -6 and -1.2 V using the same parameters that were used to fit the experimental I-V characteristics. Both plots are shown in the following Figures 11 and 12. Since the parameters were fit for a Fowler-Nordheim tunneling dominated device, the nonlinear behavior is expected. For the plot at a bias of -1.2 V, which is within the noise floor voltage range, there is a resulting offset that occurs from the noise level.

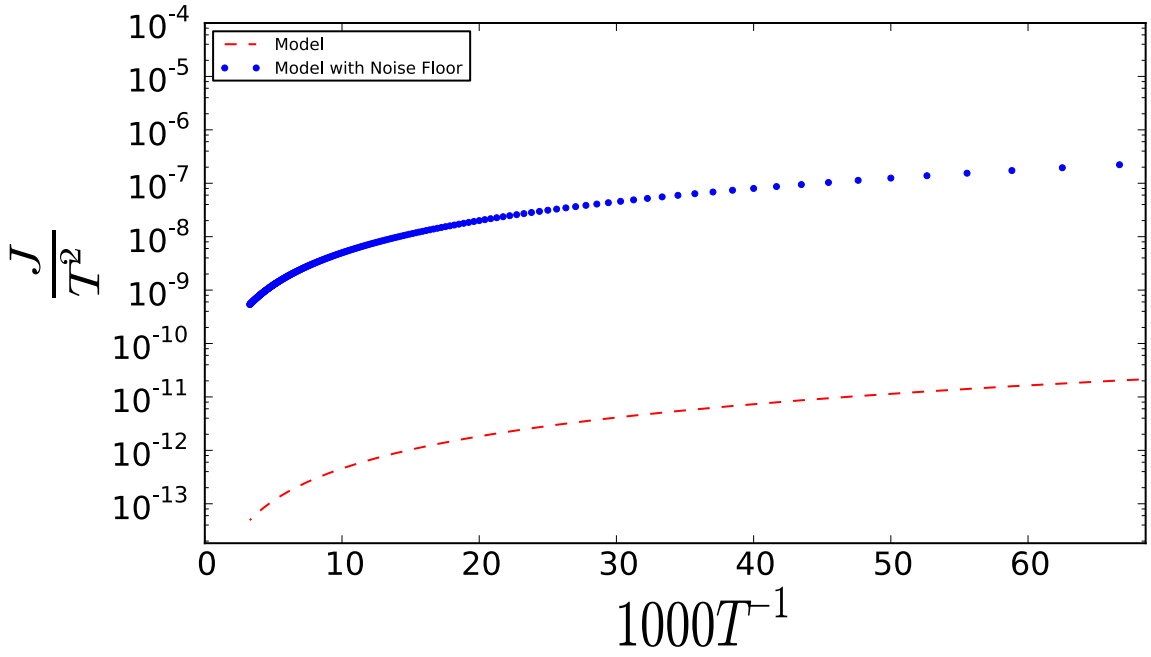

Figure 12: Simulated results of $\ln \frac{J}{T^2}$ vs. $\frac{1000}{T}$ at a bias of -1.2 V or an electric field of -1.2 MV/cm. The red shows the original simulated result while the blue shows the simulation with a noise floor, resulting in an offset that results from the current magnitude being equal to the noise level throughout. The behavior is non linear due to the dominance of Fowler-Nordheim tunneling and the lack of Schottky emission.

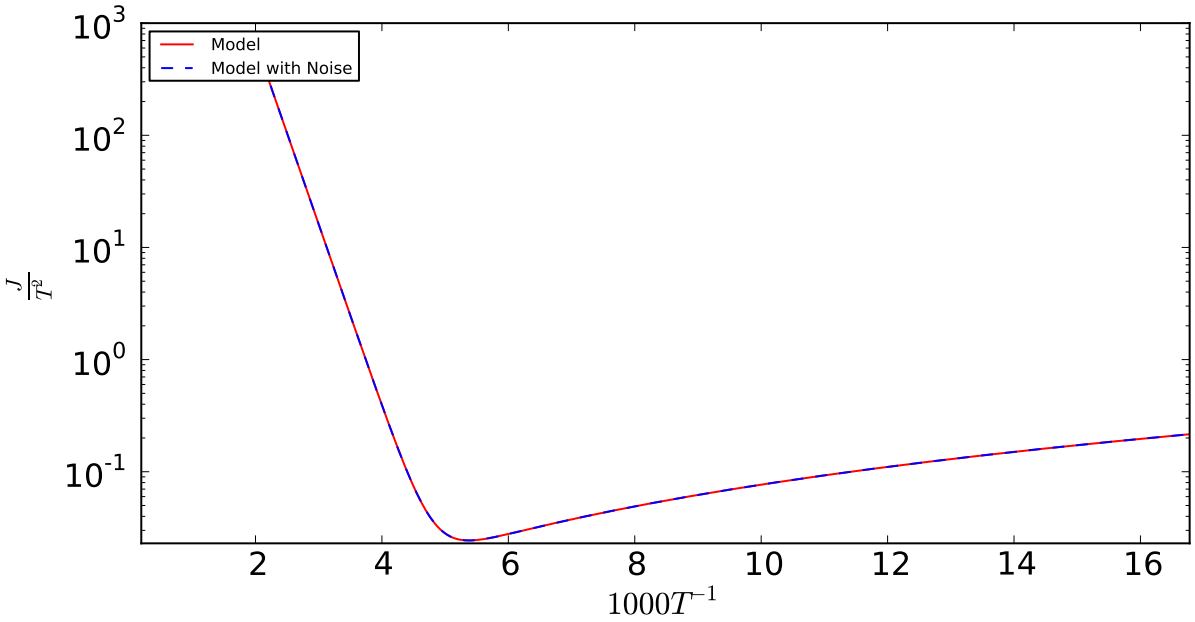

Figure 13: Simulated results of $\ln \frac{J}{T^2}$ vs. $\frac{1000}{T}$ at a bias of -1.2 V or an electric field of -1.2 MV/cm using parameters that display the effects of thermal effects. The red shows the original simulated result while the blue shows the simulation with a noise floor, which in this case are the same. Above an onset temperature at which a local minimum occurs on the plot, the behavior becomes linear due to the domination of Schottky emission over the tunneling current.

To illustrate the expected behavior of a device dominated by thermal effects, Figure 13 shows $\ln \frac{J}{T^2}$vs. $\frac{1000}{T}$ plot repeated with the thermal effects dominated barrier height values of 0.5 eV (M_1/I) and 0.7 eV (M_2/I) at the metal-insulator interfaces as well as an effective mass ratio of 1. The device is expected to be under great influence of Schottky emission conduction at a bias of -1.2 V. The results show the expected linear behavior at higher temperatures, where Schottky emission dominates. There is a local minimum that marks the transition of the dominant conduction mechanism.

4.4 Fowler-Nordheim Tunneling

Plotting $\ln\frac{J}{E^2}$ against $\frac{1}{E}$ of both simulated and experimental results in Figure 14, a near linear trend is only shown to be for higher electric fields, where the Fowler-Nordheim tunneling current is expected to be dominating. The noise floor cuts out a portion of the linear region, producing an artificial plateau region with an elbow, but becase the current quickly rises above the noise floor under Fowler-Nordheim tunneling dominance, the noise floor masks mostly the non-tunneling region at low biases. Additionally, the simulated results suggest that the overall behavior is more than a simple linear behavior in the Fowler-Nordheim dominated regions despite the more linear behavior of experimental results above the noise floor. Again an offset is observed between the simulated and the experimental data in the positive bias results as a result of the discrepancy between experimental and simulated I-V response for that side.

For comparison, the same plot was simulated using 0.5 and 0.7 eV as barrier height values for a device at 500 K with an effective mass ratio of 1 to produce the expected non-linear behavior of a device dominated by thermal effects, shown in Figure 15.

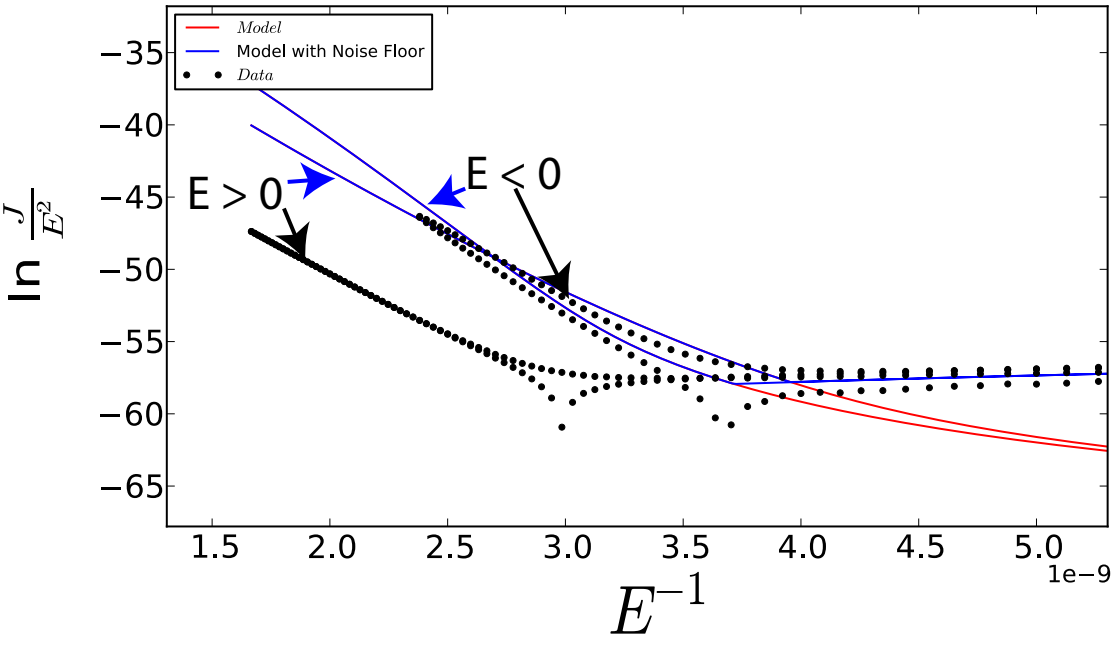

Figure 14: Simulated and experimental results of $\ln \frac{J}{E^2}$ vs. $\frac{1}{E}$. The red shows the original simulated result while the blue shows the simulation with a noise floor and the black show the experimental results. The linear like behavior appears at the higher electric fields, marked by when the current rises above the noise floor.

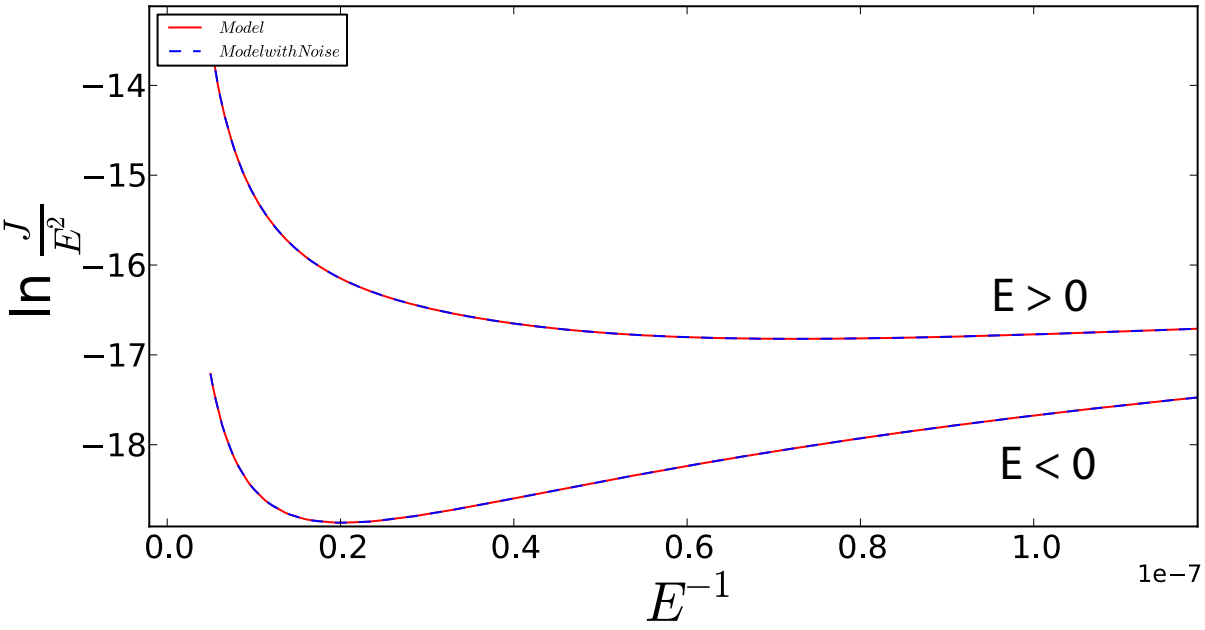

Figure 15: Simulated results of $\ln \frac{J}{E^2}$ vs. $\frac{1}{E}$ with thermal effects dominated parameters.. The red shows the original simulated result while the blue shows the simulation with a noise floor. The linear like behavior seen in Figure 14 is less prevalent in this plot. However, at higher biases, the curves can be taken for possessing linear trends.

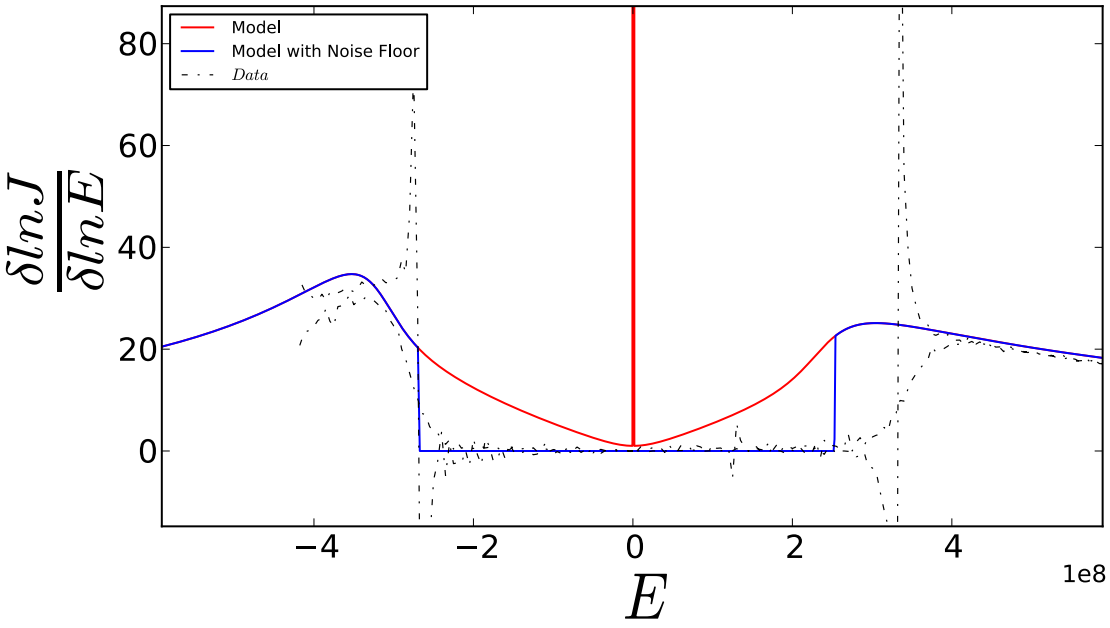

Figure 16: Simulated and experimental results of $\frac{d\ln J}{d\ln E}$ vs. E . The red shows the original simulated result while the blue shows the simulation with a noise floor and the black show the experimental results. The noise level simulation seems to suggest the noise floor interfering with the analysis. The offset at the positive bias is again due to the non-matching I-V characteristics of the experimental result with the simulations. The spikes in experimental data are a result of the displacement current in the I-V response during the reverse sweep back to 0 V.

Plotting $\frac{d\ln J}{d\ln E}$ vs. E in Figure 16 as according to Murakami, the peak characteristics expected of tunneling dominated devices are observed. However, the plotted experimental results are obfuscated by noise and displacement currents which cause the spikes, and provide a poor concrete indication of the behavior.

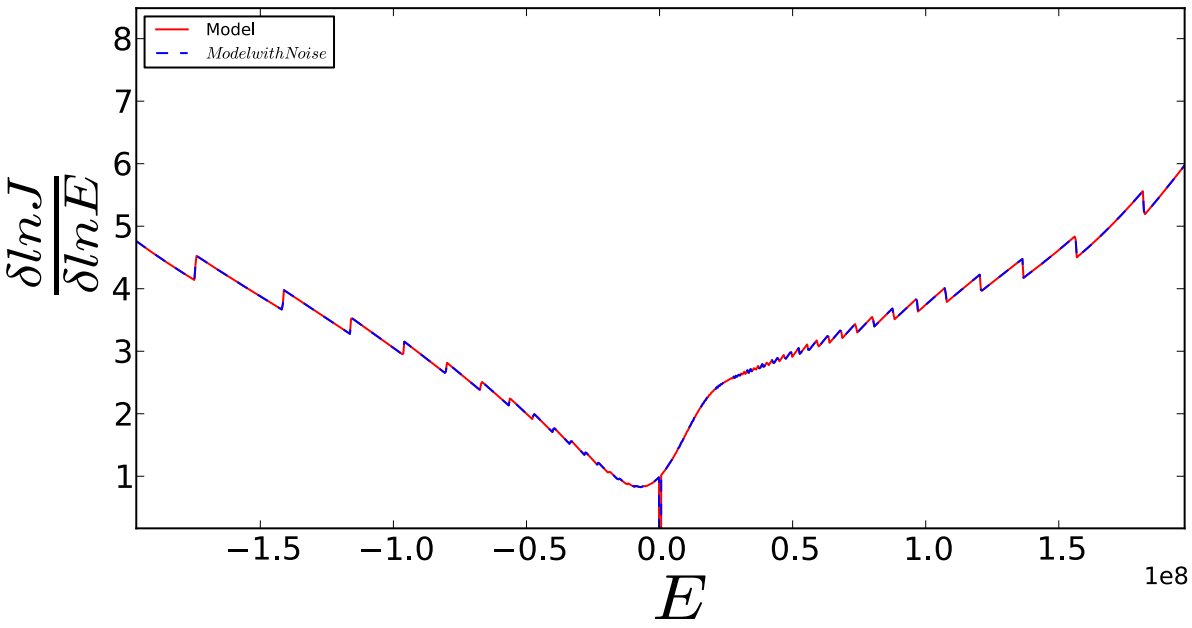

Figure 17: Simulated results of $\frac{d\ln J}{d\ln E}$ vs. E in thermal effects dominated parameters. The red shows the original simulated result while the blue shows the simulation with a noise floor, the two which in this case are the same. As expected, there is a lack of distinct peaks that would appear if the device was under the influence of Fowler-Nordheim tunneling. The teeth are an artifact of the simulation.

Additionally, the same plot was simulated using 0.5 eV (M_1/I) and 0.7 eV (M_2/I) as barrier height values for a device at 50 and 500 K with an effective mass ratio of 1 to produce the expected behavior of a device dominated by thermal effects in Figure 17. The plots lack the peak shown in the previous plot, due to the dominance of thermal effects over Fowler-Nordheim tunneling, and the peaks reappear when the temperature is dropped down to 50K in Figure 18.

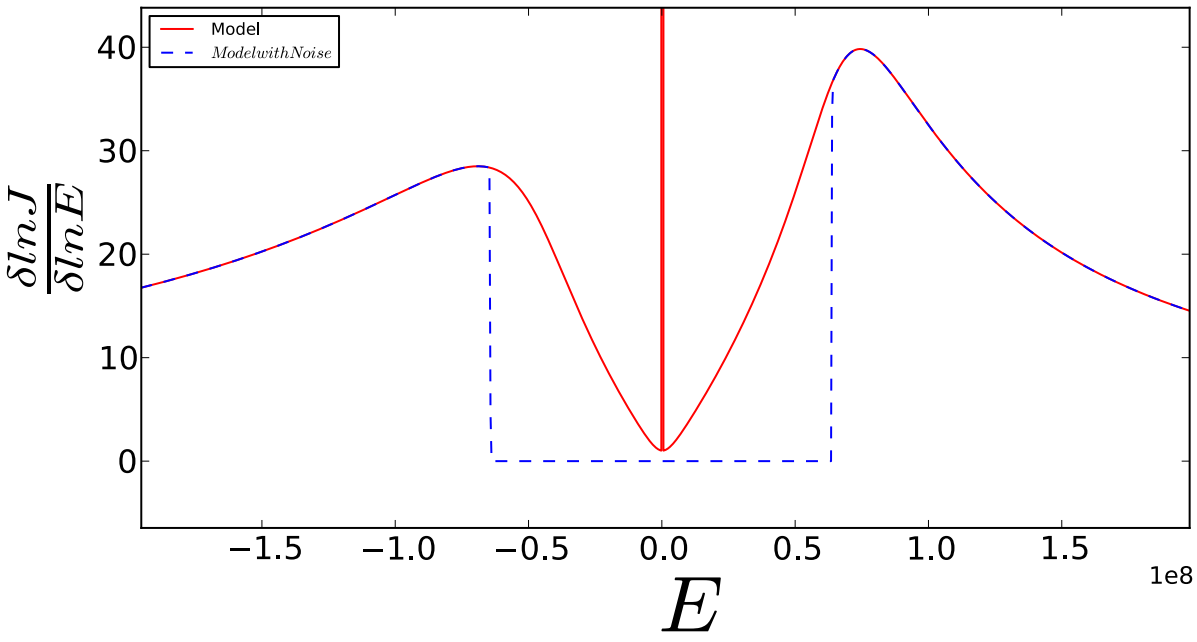

Figure 18: Simulated results of $\frac{d\,ln\,J}{d\,ln\,E}$ vs. E with the same parameters as Figure 17 save the temperature, which has been lowered to 50 K. The red shows the original simulated result while the blue shows the simulation with a noise floor. The effects of the noise floor have to be considered as the overall current response drops due to the lower thermionic response at a temperature of 50 K. As a result, the distinct peaks in the plot re-appear, signifying that Fowler-Nordheim tunneling is the dominant mechanism at this temperature.

4.5 Temperature Variations

Devices with smaller barrier heights tend to see a shift in the voltage at which the peak of the logarithmic conductivity analysis occurs as the temperature is increased. This is due to the dominance of thermal effects current over the the tunneling current in the device as the temperature increases. Beyond certain temperatures, the peaks are completed buried in the current response, showing logarithmic conductivity analyses are only applicable for tunneling dominated devices. The two Figures 19 and 20 show the results of simulation with barrier heights of 0.5 eV (M_1/I) and 0.7 eV (M_2/I) for the two metal-insulator interfaces, an effective tunneling mass ratio of 1 , a thickness of 10 nm, a high frequency dielectric constant of 1.3, at two different temperatures of 50 K and 500 K. At 50 K, both peaks are still visible whereas at 500 K the peaks have been completely flooded out.

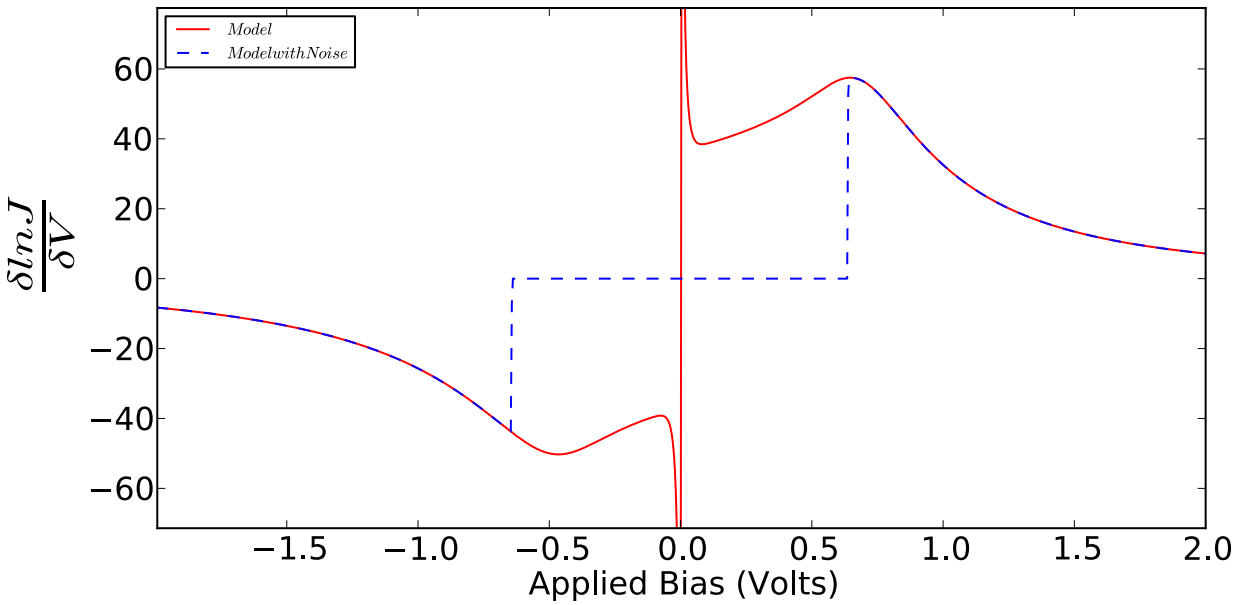

Figure 19: Simulated results of $\frac{d\,ln\,J}{dV}$ vs. V at 50 K. The red shows the original simulated result while the blue shows the simulation with a noise floor. The noise level simulation seems to suggest the noise floor interferes with the analysis, producing peaks at voltages that may be mistook for barrier height values. The distinguished peaks show that Fowler-Nordheim tunneling is the dominant mechanism.

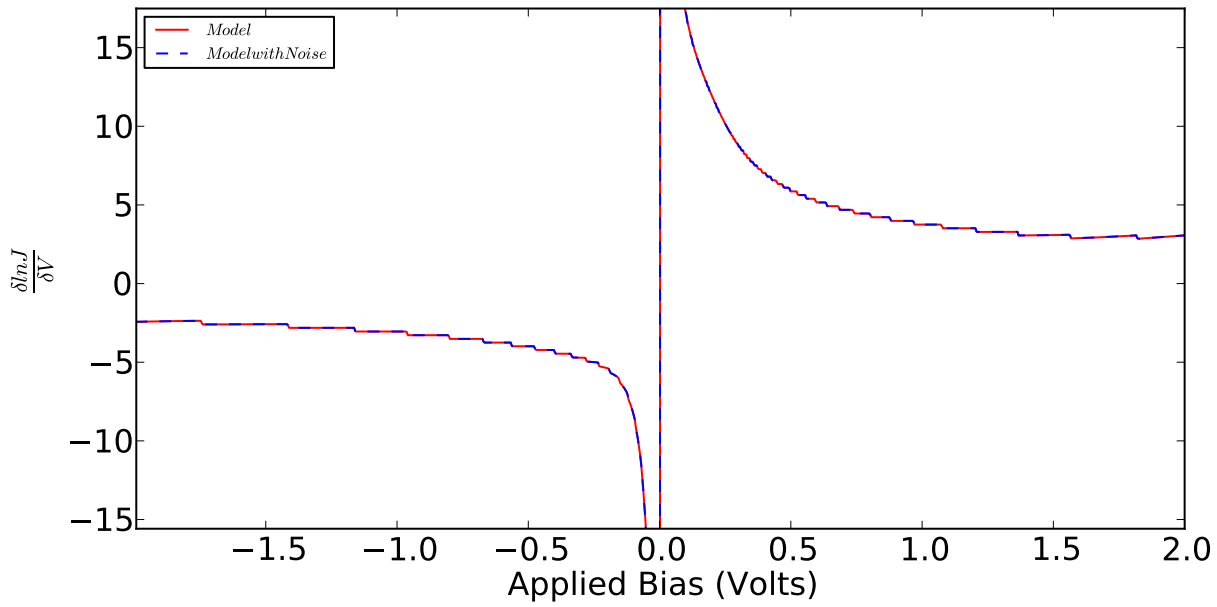

Figure 20: Simulated results of $\frac{d\ln J}{dV}$ vs. V at 500 K. The red shows the original simulated result while the blue shows the simulation with a noise floor. Contrary to Figure 19, there are no peaks observable in this plot due to thermal effects.

The shift is observed in Figure 21, which plots the voltage at which the local maximum occurs against the temperature simulated. The dominance of thermal effects increases the bias at which the maximum occurs until the peak is indistinguishable. For the interface with the larger barrier height, this occurs at higher temperatures.

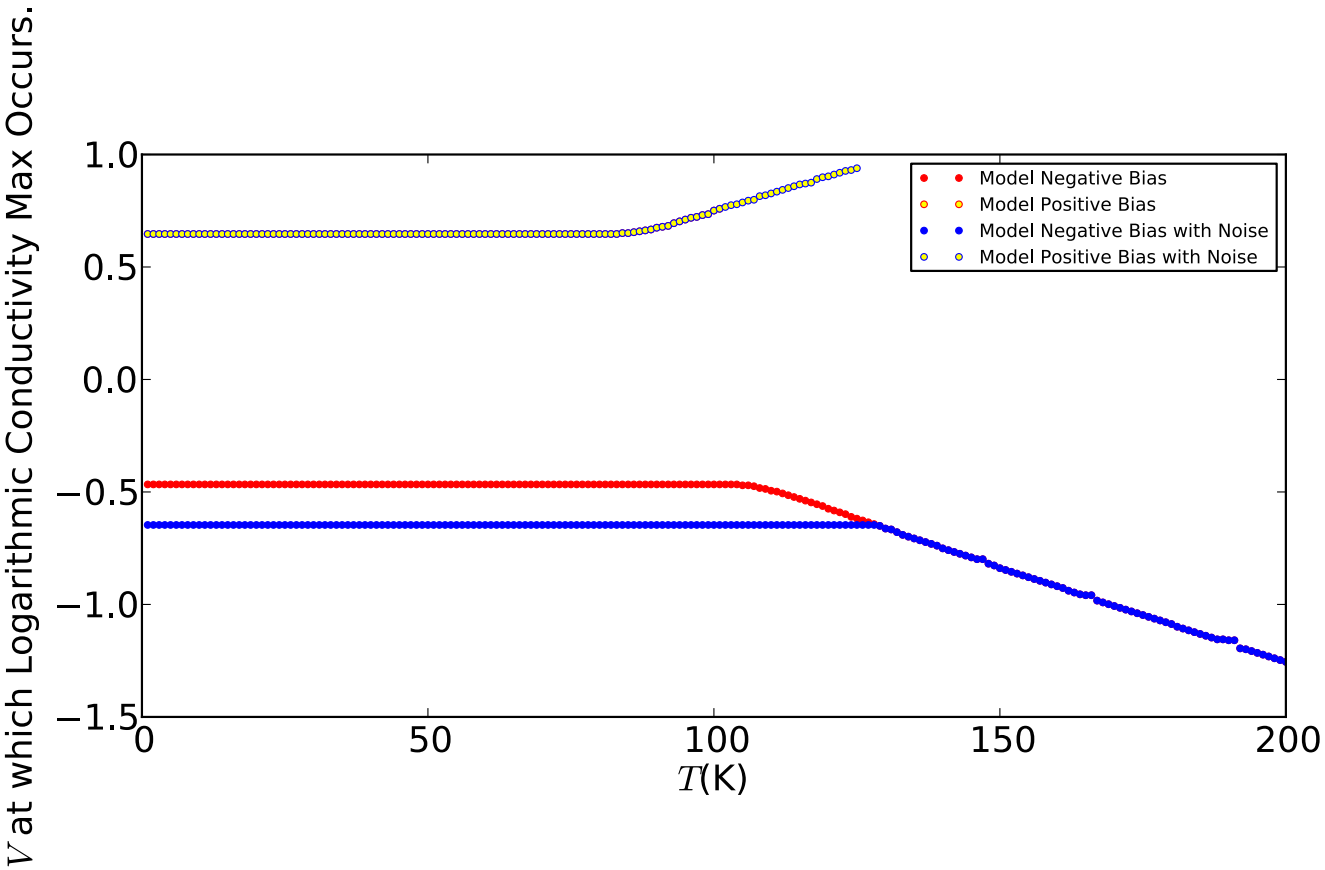

Figure 21: Simulated results that track the voltage values at which the peak value occurs for the $\frac{d\ln J}{dV}$ vs. V plot as a function of temperature. The red shows the original simulated result while the blue shows the simulation with a noise floor, both positive and negative bias responses are shown on this plot. As shown above, there are three states. First, a plateau that exists at lower temperatures. This is where the analysis method is able to correctly identify barrier height values in the device structure if there are no interferences from the noise floor. Second, there is a linear region where the thermal effects start to take over and gradually shift the peaks away from the correct barrier height values. This occurs until the third state, where peaks have either shifted outside of the voltage range simulated or disappeared altogether as the device is entirely dominated by thermal effects. Another observation from this plot is how the noise level can throw off the barrier height approximation results even when there are no thermal effects, shown by the negative bias results (solid blue dots).

5 Summary

In this work, I-V responses of MIM tunnel junctions were simulated with various parameters to model devices operating under Fowler-Nordheim tunneling dominated parameters and thermionic emission dominated parameters. The I-V responses were then plotted according to analysis techniques in literature in order to extract device characteristics, and results were compared to understand how techniques differed depending on the dominant conduction mechanism. Additionally, to observe the effect of temperature on the analysis results, various measurement temperatures were simulated for the MIM device. A noise floor was also simulated in order to examine its effect on the variety of analysis plots. Such simulations showed the interference of the noise floor in the plot of $\frac{d\,ln\,J}{d\,ln\,E}$ vs. E as well as with the logarithmic conductivity analysis. The interferences show how mistaken barrier height values can be extracted from the graph if the analyzer is not careful. The noise floor is also shown to produces artificial plateau like behavior in a variety of analyses, in addition to the logarithmic I-V response. Such behavior, in conjunction with Fowler-Nordheim tunneling, can create curves that look linear at higher biases due to the lack of information at lower biases. The curves may be mistakenly taken to be results of a thermal effect dominated device. The voltages at which the logarithmic conductivity peaks occur are also shown to be linearly increasing when the temperature rises as thermal effects are more dominant. Within the same voltage range, the same device can yield distinguishable peaks at lower temperatures and not at higher temperatures. Additionally, this work compared the simulated results against experimental data analyses, yielding behaviors that were similar qualitatively but quantitatively different, suggesting factors that were not considered in the simulation, though some differences may have been a result of a native zirconium oxide layer on the ZCAN and AlOx interface. Such a native oxide may increase the effective thickness for tunneling from the ZCAN to the Al, lowering the experimental current.

References

[1] P. C. D. Hobbs, R. B. Laibowitz, F. R. Libsch, Appl. Optics, 44 (2005) 6813

[2] R. H. Fowler, L. Nordheim, Proc. R. Soc. London, Ser. A 119 (1928) 173.

[3] J. G. Simmons, J. Phys. D: Appl. Phys. 4 (1971) 613.

[4] J. Frenkel, Phys. Rev. 54 (1938) 647.

[5] P. R. Emtage, and W. Tantraporn, Phys. Rev. Lett. 8 (1962) 267.

[6] J. G. Simmons, J. Appl. Phys. 34 (1963) 2581.

[7] R. G. Southwick III, A. Sup, A. Jain, W. B. Knowlton, IEEE T. Device Mat. Re. 11 (2011), 236.

[8] K.H. Gundlach, and J. Holzl Surf. Sci. 27 (1971) 125.

[9] J.G. Simmons, Phys. Rev. 155 (1967) 657.

[10] J.G. Simmons, Phys. Rev. 166 (1968) 912.

[11] T.E. Stern, B.S. Gossling, and R.H. Fowler, Proc. R. Soc. London, Ser. A 124 (1929) 6.

[12] K. Murakami, M. Rommel, V. Yanev, T. Erlbacher, A. J. Bauer, L. Frey, J. Appl. Phys. 110 (2011) 054104.

[13] T. O'Regan, M. Chin, C. Tan, and A. G. Birdwell, ARL-TN-0464 (2011).

[14] N. Alimardani, E. W. Cowell III, J. F. Wager, J. F. Conley Jr., D. R. Evans, M. Chin, S. Kilpatrick, M. Dubey, Vac. Sci. Technol., A 30, (2012) 01A113.

[15] E. W. Cowell, N. Alimardani, C. C. Knutson, J. F. Conley, Jr., D. A. Keszler, B. J. Gibbons, and J. F. Wager , Adv. Mater. 23, (2011) 74.